Cracking shells and scrambling eggs: intermediate shell formation and anion rearrangement in the cation exchange from π-SnS to $Cu_{1.8}S$

Suresh Sarkar,[1†‡] Christopher. G. Sharp,[1‡] Shane T. Finn,[1†] and Janet E. Macdonald.[1, 2*]

[1] Department of Chemistry, Vanderbilt University, Nashville, TN, 37235, USA.

[2] Vanderbilt Institute of Nanoscale Science and Engineering, Vanderbilt University, Nashville, TN, 37235, USA.

KEYWORDS: tin(II) sulfide, copper(I) sulfide, nanocrystal, cation exchange, polytype, Kirkendall effect

ABSTRACT: Cation exchange is used to achieve products of complex morphology, phase or elemental compositions from host particles with similar features. Understanding which parameters are responsible for preserving or altering these features is key to predicting novel cation exchange products. Here we demonstrate cation exchange of cubic π-SnS to pseudo-hexagonal roxbyite ($Cu_{1.8}S$) as confirmed by powder X-ray diffraction, transmission electron microscopy and Energy Dispersion Spectroscopy mapping. TEM/EDS shows the initial formation of a shell of amorphous Cu-Sn-S. It is only upon elevated temperatures that the shells are breached on one facet and complete cation exchange to a copper sulfide core occurs. Mismatched diffusion rates between the outgoing Sn^{2+} and the in-coming Cu^{+} cause the formation of voids in the cation exchanged nanocuboids; a documented result of the Kirkendall effect. These mismatched rates are implicated in the change of the sulfide lattice from pseudo-fcc to pseudo-hcp. The prepared nanocrystals were studied as photoabsorbers in Quantum Dot Sensitized Solar Cells (QDSSCs) and found that shelling of the π-SnS with the amorphous Sn-Cu-S does not greatly change the cell characteristics or performance indicating that the voltage limiting defect in π-SnS solar cell designs is in the core, not the surface of the material.

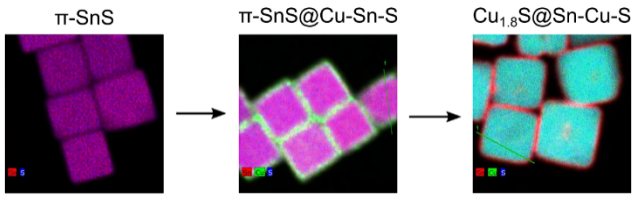

Polytypism in crystal systems has been shown to alter the properties of materials without change in elemental composition.[1,2] Of note are the II-VI semiconductors, which are well studied in both their known thermodynamic and metastable phases, such as the wurtzite/zincblende polytypism of CdS and CdSe quantum dots which offer differing optoelectronic properties based on crystal structure.[3–6] Similar cubic/hexagonal polytypism has been seen in unexpected places, where only one phase is known in the bulk.[7–10] The extreme kinetic trapping afforded by nanoscale synthesis and the large surface energies capture and stabilize these metastable phases.[11,12] Recent synthetic efforts have explored the tunability of nanoscale materials and the conditions necessary to achieve specific product phases to gain further control over material properties, especially in crystalline materials with complicated phase spaces.[7,13–15]

In addition to several compositionally different phases, the I-VI semiconductors show cubic/hexagonal polytypism in their I_2-VI composition, some of which are already seen in mineral phases. Notable examples include the silver and copper chalcogenides which each possess several different phases of differing stoichiometry and where Cubic/Hexagonal polytypism further diversifies their resulting properties and potential application.[16,17] Nanomaterials of these semiconductors possess potential applications in thermo- and opto-electronic applications while often being comprised of abundant and environmentally friendly precursor reagents.[18,19] The copper chalcogenides have been of particular interest, due to the ion mobility of copper lending products to a wide number of stoichiometries, each with their own unique properties.[9] This ion mobility has been further explored post-synthetically, with copper seeing use as either a leaving or entering body during cation exchange.[9,13,20,21]

These principles of ion mobility have seen popular use as a route towards non-standard phases through cation exchange, and less commonly anion exchange.[22,23] The ability to remove and replace ions with varying stochiometric ratios while leaving the counterions undisturbed have led to a wide variety of novel material synthesis.[24] Of particular note are uncommon hexagonal phases which have been sought due to the unique traits which stem from anisotropic crystal lattices. The Schaak group has demonstrated this using numerous different cations towards similarly arranged wurtzite products stemming from hexagonally packed roxbyite $Cu_{1.8}S$ as host particles.[9]

Retention of the anion sublattice structure in cation exchange is oft touted as an underpinning principle of cation exchange, and that the sublattice of the host material can be a predictor of the phase of the products.[25] Exceptions where the anion sublattice is not retained can occur. Strongly unfavorable thermodynamics of the product affect anion

retention. Examples includes the cation exchange of Cu_2S to bcc Au_2S, and also the exchange of hexagonal Cu_2S to rock salt PbS,[26] for which there is no known hexagonal phase.[13]

Where polytypism is possible, ligands are usually implicated as a phase directing agent. Ligands have a complex relationship with phase control and three different mechanisms have been identified. Ligands can manipulate the exchange kinetics of the cations. Unbalanced flow of cations in and out of the host lattice can cause collapse to a thermodynamic phase of the product. An example was the manipulation of copper ion availability through phosphine- and amine-binding ligands to alter exchange kinetics, which allowed for a gradient between two phases to be achieved during cation exchange of Cu_2S to $CuFeS_2$.[7] Ligands can also remove anions from the host material changing the phase of the host *in situ*, as was seen recently in the exchange from cubic $Cu_{1.8}S$ to ZnS. Trioctylphospine removed sulfur from the lattice of the copper sulfide to create a tetragonal Cu_2S intermediate.[27] Lastly, alteration of host thermodynamics using surface stabilizing ligands to change the ion lattice phase during and post-synthesis is a well-established process.[6,28]

Our research seeks understand the synthetic parameters necessary for nanomaterial phase control and stability with the aim of further expanding the existing library of products not found in the bulk scale. Here we add to this knowledge the cation exchange *to* copper sulfide from cubic phase π-SnS nanocrystals. Copper sulfide is chosen because there several known pseudo-hexagonal and pseudo-cubic phases. While exchange from hexagonal phases such as wurtzite CdS to hexagonal phase $Cu_{2-x}S$ are established, cation exchange from cubic phases is underexplored. Interestingly, the copper sulfide product here, from a cubic phase SnS, is pseudo-hexagonal roxbyite ($Cu_{1.8}S$), which is peculiar due to there being and the established body of literature emphasizing sublattice preservation as the key parameter in controlling the product phase in cation exchange reactions.

Through careful characterization and experiments that seek reaction intermediates, an intermediate product with an amorphous shell of Cu-Sn-S is identified as an important factor in the kinetics of the cation exchange, not the ligands.

Since π-SnS is a relatively new crystalline phase that is identified as a potentially revolutionary solar cell absorber material in tandem cell designs, we took the opportunity to study how the shell formation effects performance in the quantum dot sensitized solar cell designs.[29–31] The results suggest that the defects or semiconductor characteristics that are limiting the open circuit current of cells made with π-SnS are not located on the surface of the material.

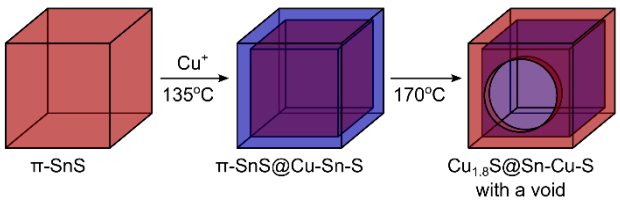

Figure 1. Schematic representation of cation exchange process.

RESULTS/DISCUSSION

π-SnS nanocuboids were synthesized following a modified literature method reported by Patra *et al.*[32] A solution of thiourea and hexadecylamine (HDA) was injected into a solution of tin(II) chloride and tributylphosphine (TBP) in HDA at 175°C. After an initial temperature drop, the solution was held at 155°C for 20 min. An aliquot of π-SnS nanocuboids was taken for characterization. Powder X-ray diffraction (XRD) confirmed predominant presence of cubic π-SnS with orthorhombic α-SnS (JCPDS# 39-0354) side product (Figure 2).[33,34] Both phases can be described as distorted rock salt structures with the sulfide anions in distorted fcc arrangements. While the distortions from ideal octahedral cation coordination in α-SnS are uniaxial and lead to sheet- and plate-like structures, the distortions in π-SnS happen in all directions, leading to an overall non-centrosymmetric, pseudo-cubic structure with a large unit cell of 64 atoms. High resolution TEM confirmed a single-crystalline product with a cuboid shape (Figure 3, edge length = 52 ± 5 nm, n = 120, S1).

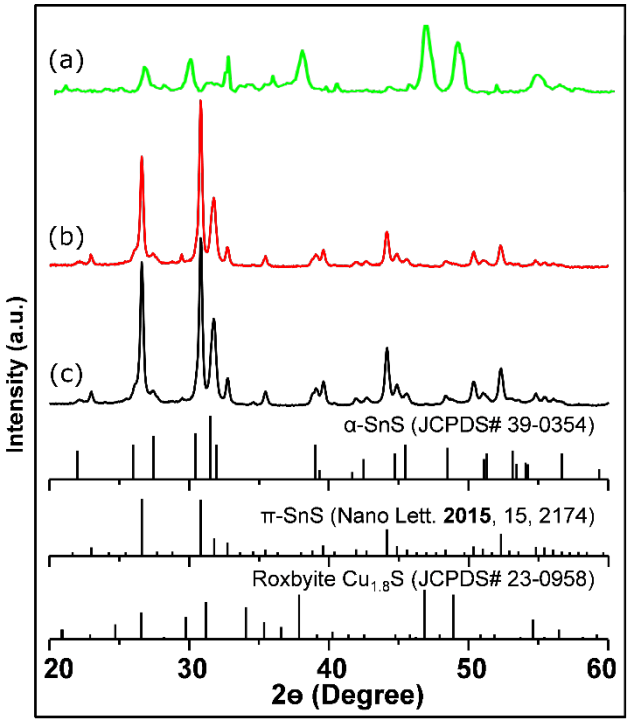

Figure 2. XRD at the different stages of the cation exchange reaction. a, b, and c are the XRD for $Cu_{1.8}S$@Sn-Cu-S, SnS@Cu-Sn-S, and pristine SnS, and, respectively.

Cation exchange was performed without purification of the SnS nanocuboids. The reaction solution was reduced to 90°C prior to an air-free injection of CuCl solubilized in oleylamine. The temperature was then ramped to 170°C. Aliquots were collected at several temperatures to observe the exchange processes (Figure 2).

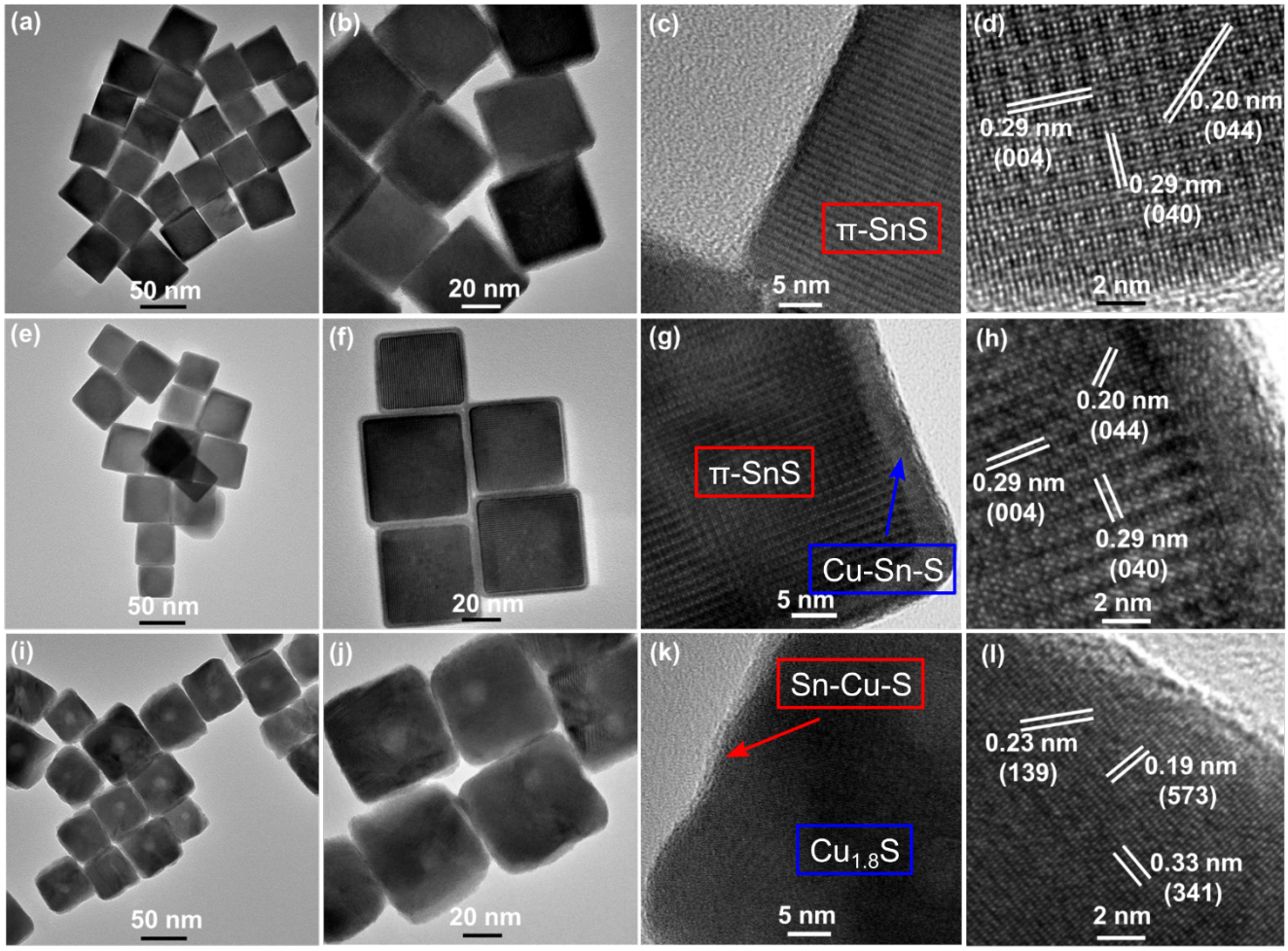

Figure 3. TEM and HR-TEM images of SnS nanocuboids (a-d), SnS@Cu-Sn-S nanocuboids collected at 135 °C (e-h) and $Cu_{1.8}S$@Sn-Cu-S nanocuboids collected at 175°C (i-l).

TEM analysis of aliquots collected after the copper injection at 135°C (52 ± 5 nm, n = 120), show similar morphology and size to the original SnS nanocuboids (Figure 3). HR-TEM shows a 4 nm amorphous shell has developed (Figure 3). Energy dispersive X-ray spectroscopy (EDS) mapping and a line scans across the cuboid indicate the particles possess a tin sulfide core with a copper rich copper-tin-sulfide shell (Figure 4), herein designated as core@shell π-SnS@Cu-Sn-S. XRD did not show additional reflections due to the shell further supporting its amorphous nature. HR-XPS suggests that the chemical environments of the atoms of the shell is close to that of the known crystalline phase $Cu^{1+}{}_3Sn^{4+}S_4$ (Figure S3). While there are several known ternary copper tin sulfide phases, we saw no evidence of a crystalline phase here.

This first stage of cation exchange to π-SnS@Cu-Sn-S is diffusion limited and self-limiting. This conclusion is drawn because even under extended heating at 135°C or high copper concentrations, the shell was not any thicker. This step is also highly favored as even the addition of excess coordinating phosphine did not slow the reactivity of Cu^+ towards the particle surface. Similar observations of core@shell nanostructures with various morphologies due to the cation exchange process (with product phase shell and pristine lattice core) have been reported.[35–38]

It was only after increasing the temperature to 170°C that extensive cation exchange of the core of the π-SnS@Cu-Sn-S was observed. EDS mapping and a line scan across the cuboids confirmed a copper sulfide core and a remaining tin rich, tin-copper-sulfide shell (Figure 5), designated herein as $Cu_{1.8}S$@Sn-Cu-S.

XRD of the product of the product of the full cation exchange shows additional reflections at 37.7°, 46.5° and 48.9° characteristic of a hexagonal-like copper(I) sulfide and was assigned to Roxbyite, $Cu_{1.8}S$. Roxbyite has a complex structure with a large unit cell but can be approximated as a simple hexagonal structure. The reflections were accordingly assigned; 37.7° is the (102)-like planes, 46.5° (110)-like planes, and the 48.9° (103)-like planes. HR-TEM showed that the particles were single-crystalline. A pair of perpendicular lattice fringes were assigned to d = 0.33 nm as (100)-like planes, and d = 0.19 nm as (110)-like planes. A third set of fringes, d = 0.23 nm, was assigned to (102)-like planes.

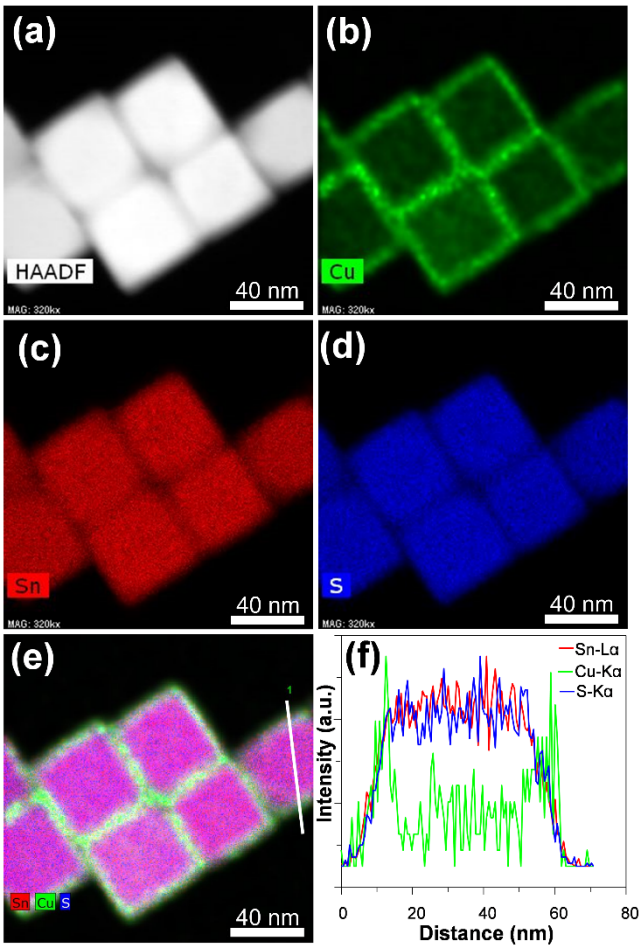

Figure 4. a) High Angle Annular Dark Field- Scanning Transmission Electron Microcopy (HAADF-STEM) image of the nanocuboids collected at 135°C (b-e) EDS elemental mapping (f) relative EDS signal of Sn, Cu and S along the line noted in (e).

The distorted hcp anion lattice of roxbyite $Cu_{1.8}S$ indicates that there is a major structural transformation from the fcc anion lattice of π-SnS upon cation exchange. Our observation contrasts with many studies on cation exchange which highlight a retention of the anion sublattice. For example, in our own work we have found, In^{3+} and Fe^{3+} exchanges into Cu_2S yields metastable wz-$CuInS_2$, rather than the thermodynamic chalcopyrite cubic-like phase.[39] The Schaak group has employed exchange of $Cu_{2-x}S$ from the cubic-like (digenite) and hexagonal-like (roxbyite) phases to zinc blende and wurtzite CoS and MnS.[7,9] They show that there is a retention of both the cation and anion lattices, as expressed in the anion stacking (ccp or hcp) and the holes (tetrahedral, not octahedral).

It is particularly intriguing that the anion lattice is not retained in the cation exchange to copper(I) sulfide as both hexagonal and cubic polymorphs are known. One might predict that the fcc lattice of rock-salt-like π-SnS in the cation exchanged with Cu^{1+}, would yield cubic $Cu_{2-x}S$ digenite, anilite or geerite (all have fcc anion lattices, with slightly different cation placement and vacancy orderings). Digenite, in particular, has been isolated in nanocrystals previously, is stable above 73°C, and metastable at room temperature.[40] It should be noted that there is a small lattice mis-match of less than 8% in this system despite the large change in cation radius (Cu(I) ~77 pm and Sn(II) ~118 pm).[41] The pseudo-close packed directions have lattice spacings of 3.58 Å for roxbyite of 3.22 Å for digenite and 3.35 Å for π-SnS.[42,43] Therefore large lattice mis-match cannot be implicated for phase changes.[13] Furthermore, the activation energy for the transformation of digenite into a hexagonal phase such as roxbyite, is high requiring temperatures between 300 and 400°C; such a transformation requires the presence of defects and extensive slip planes.[44,45] The cation exchange processes likely induces the required defects for such a transformation.

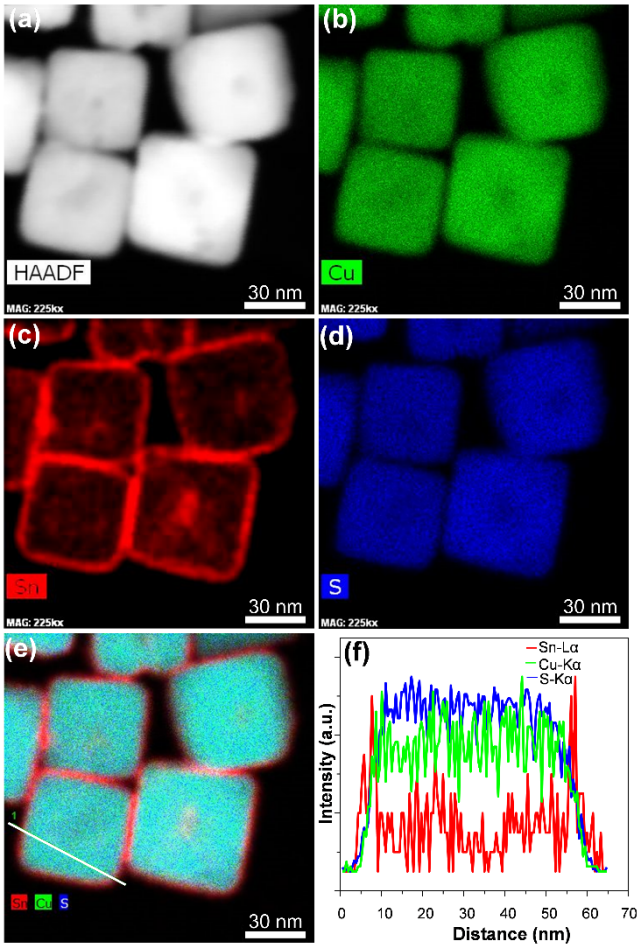

Figure 5. a) HAADF-STEM image of the nanocuboids collected at 170°C (b-e) EDS elemental mapping (f) relative EDS signal of Sn, Cu and S along the line noted in (e).

A plausible reason for the rearrangement of the anion lattice to yield the thermodynamic product mis-matched rates of ion diffusion which cause the transient formation of phase- change catalyzing defects. A similar phenomenon was seen in the phase-controlled exchange of hexagonal-Cu_2S to $CuFeS_2$.[7] When the rates of Cu^{1+} removal and Fe^{3+} incorporation were matched, the hexagonal lattice of the host material was maintained to yield metastable wurtzite-like $CuFeS_2$. When the Fe^{3+} incorporation was hindered by strongly coordinating ligands in solution, the lattice transformed to the thermodynamic cubic phase $CuFeS_2$. It was hypothesized that transient defects caused by cation deficiencies were necessary to catalyze the lattice transformation.

In the experiments here, when π-SnS@Cu-Sn-S particles underwent complete cation exchange to $Cu_{1.8}S$@Sn-Cu-S, there resulted noticeable voids in material, usually on one face (though the size of the overall structure remains similar to the host (52 ± 5 nm, n = 120)), Such voids are a hallmark of the Kirkendall effect (Figure 6, S13) of slow diffusion inwards compared to diffusion outwards.[20,22,23,46] Study of samples in which only some particles had undergone complete exchange are illuminating. While some pitting of the shells are observed in the π-SnS@Cu-Sn-S particles that remained, the large voids were exclusively, and consistently observed in particles that had undergone exchange (Figure 7). This suggests that the voids are formed from the speedy diffusion of tin out of the nanostructures compared to the copper incorporation. Buhro et al. also observed a similar case of hollow formation at the interior of $CuInS_2$, while performing the diffusion of In^{3+} into $Cu_{(2-x)}S$, and has predicted that the fast outward diffusion of Cu^+ relative to the inward diffusion of In^{3+} causes the material to erode from the center of the nanodisks.[20] Here, the opposite is seen where the copper has slow diffusion compared to the Sn. This remarkable as both the cubic-like and hexagonal-like copper(I) sulfides have high cation mobilities at temperatures over 100°C.[47,48] Why, therefore, is the inward copper diffusion slow in this system?

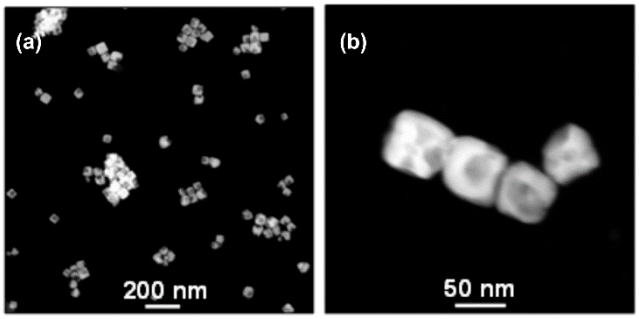

Figure 6. High-angle annular dark-field (HAADF) imaging of $Cu_{1.8}S$@Sn-Cu-S nanocubes illustrating the voids in the structure.

Clues to the mechanism of the transformation came through the attempts to capture intermediates of the cation exchange reactions. Other have used these intermediates to understand the dominating epitaxial relationships between the two phases can be observed, and the crystallographic "directions of attack" can be deduced.[41,49–51] The Manna group has studied the conversion of particles with cubic-like crystal structures of Cu_2X to cubic- SnX (X= Se or Te). In both cases, the exchange was gradual and the heterostructured intermediates contained crystalline domains of each species. While core-shell structures could be obtained, they were metastable and resolved to Janus-type structures at higher temperatures.[35,49,52]

In an attempt to capture cation exchange intermediates in this reaction, aliquot studies, lower Cu^+ concentrations, lower reaction temperatures (Figure 7, S4-S7, S14) and different sizes of host particles (Figure S9) were attempted. Others have previously observed striped or patchy Janus-type particles as intermediates.[46,50,53–56] However, such structures were not readily observed. While both cubic and tetragonal Cu-Sn-S phases are known, no ternary structures were captured. Instead, we observed individual particles that had completely exchanged to $Cu_{1.8}S$@Sn-Cu-S, while others remained intact as π-SnS@Cu-Sn-S (Figure 7, S14). In the thousands of particles imaged across more than 50 samples, only two particles demonstrated hemispheres of $Cu_{1.8}S$ and SnS in the core. (Figure S10) – This was seen on exchange of small, ~20 nm SnS that were near spherical, and lacked the strong faceting seen in the larger particles. It is likely these smaller particles contained internal defects that prevented complete exchange.

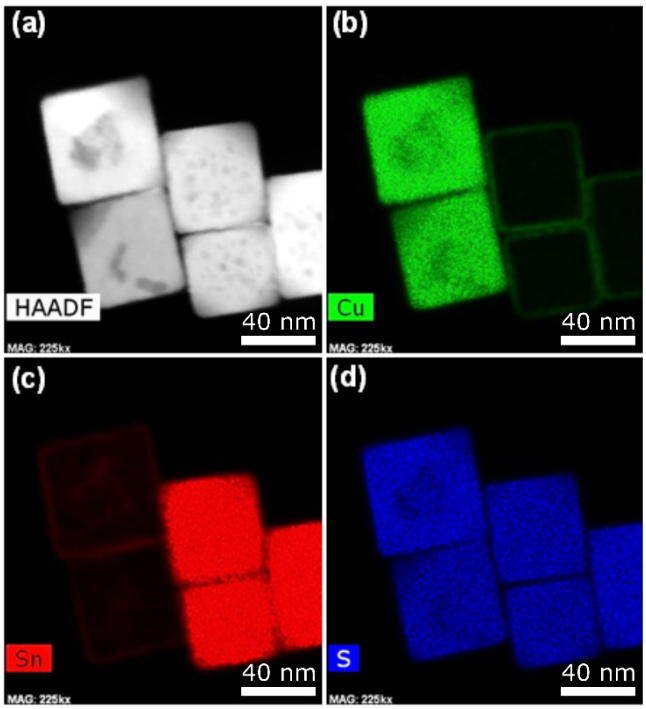

Figure 7. (a-d) EDS elemental mapping of an aliquot collected at 155°C.

The inability to capture intermediate structures suggests that once cation exchange is initiated in each particle, the reaction is rapid and complete. Jain has observed and noted cooperative mechanisms for cation exchange from CdSe to Ag_2Se and Cu_2Se.[57] The initial diffusion of the first guest cation catalyzes the incorporation of further cations. As a result, after surpassing the activation barrier of the initial diffusion of the first cation, individual particles undergo an avalanche of cation exchange, leaving other particles yet untouched. A theoretical model proposed by Ott et al. suggests that the cooperative mechanism results from, in part, coulombic interactions resultant from the differing valences of the host Cd^{2+} and guest Ag^+ cations.[58] We more recently observed a cooperative mechanism in the cation exchange of Cu_2S to $Cu^{1+}Fe^{3+}S_2$.[7] Cation charge is not the only factor that leads to cooperative mechanism as the exchange of CdS to Cu_2S does not occur through a cooperative mechanism, and instead Janus intermediates can be obtained. Therefore, it leaves additional questions as to the additional factors that lead to cooperative exchange of SnS to $Cu_{1.8}S$.

Judging by the ratio of exchanged to non-exchanged particles, the event that catalyzes the cation exchange happens more often with smaller particles and higher reaction temperatures. While some cubes will exchange at lower temperatures, even with extended annealing time (1 h), not all of the cuboids to convert to $Cu_{1.8}S$@Sn-Cu-S (Figure S8). For

smaller nanocuboids (23 ± 2 nm, n = 120), some had undergone complete cation exchange to $Cu_{1.8}S$@Sn-Cu-S at the low reaction temperature of 120 °C, but again, high temperatures of 170 °C were required to fully transform the assembly. Because there isn't one universal onset temperature for small particles and an another for large, each particle has its own "activation barrier" that is likely related to the locally variable structure and composition of the amorphous Cu-Sn-S, shell. It should be noted that the core/shell structures and voided particles decompose when the exchange mixture is brought to high temperatures of 300°C. The product is a mixture of chalcocite and CuSn (bronze) alloy particles (Figure S15, S16).

The chemical potential of copper is also important to initiate the full cation exchange. For instance, upon increasing the Cu^{+}: Sn^{2+} ratio from 5:1 to 7.5:1, complete conversion to $Cu_{1.8}S$@Sn-Cu-S at a temperature lower than that of the optimized case (detail in Figure S11).When the amount of copper-coordinating TBP was increased from 1.0 to 1.5 mL, the cation exchange processes was inhibited.[59] Only π-SnS@Cu-Sn-S nanocuboids were observed even after heating to 170°C (Figure S12). It can be hypothesized that the global cation exchange event is catalyzed by the amorphous Cu-Sn-S being breached by reactive copper ions through local weaknesses. Since the products particles each have a distinctive void centered on a face, one way to visualize the process is the Cu-Sn-S shell rupturing under pressure from copper trying to diffuse into the core and breaching the Cu-Sn-S shell. The rupture on one facet triggers a rapid loss of Sn^{2+} while stoichiometry dictates that nearly twice as much Cu^{1+} more slowly diffuses in through the same aperture under the current of escaping Sn^{2+}.

π-SnS has been identified as a new-solar cell absorber material with its band gap of ~1.7 eV, which is significantly larger than the 1.3 eV band gap of α-SnS. π-SnS should therefore give cells with a larger photovoltage than α-SnS and could be incorporated into tandem cells designs. However, to date, π-SnS has been underperforming, yielding photovoltages of under 217 mV in functioning cells.[30,31,60] While the reason is yet unclear, it can be hypothesized there is carrier trapping into defects. Here provides a convenient opportunity to test whether those defects are in the core or at the surface of the π-SnS; the products here are highly faceted, and the intermediate cation exchange products have very uniform 4 nm shells of Cu-Sn-S.

To illustrate how the amorphous mixed metal shell effects the photo responses of π-SnS, comparative photovoltaic performance of the pristine π-SnS, π-SnS@Cu-Sn-S and $Cu_{1.8}S$@Sn-Cu-S core-shell nanocuboids were measured. The particles were tested (Figure 8) as a photoabsorber materials in Quantum Dot Sensitized Solar Cells (QDSSCs) prepared according to previous work,[61] with the general structure of FTO/TiO_2/nanocrystals/ZnS/polysulfide/MoS_2/Mo.

QDSSCs prepared with π-SnS nanocrystals had a larger V_{oc} of 367mV and a marginally better fill factor of 39% than a reported thin film cell of FTO/TiO_2/pi-SnS/CdS/ZnS/ITO (217mV and 34%), but underperformed greatly in terms of the J_{sc} (0.84mA/cm² vs 5.4 mA/cm²).[30,31,60] The poor J_{sc} is likely due to design differences in the thin film and QDSSCs changing the quantity of material absorbing light, and lower driving force for charge separation across the whole system. Conversely, better potential alignments through the QDSSC system with fewer voltage losses compared to the existing thin film designs can explain the improved V_{oc} and is record-breaking for π-SnS solar cell designs.[30,31,60]

When the shell of Cu-Sn-S was added to the π-SnS, there was only a small decrease in the V_{oc}. This is evidence that the defect or inherent semiconductor characteristic that leads to the universally poor V_{oc} in existing π-SnS solar cell designs is not surface-based, but rather in the core of the material. The increased fill factor, between π-SnS and π-SnS@Cu-Sn-S suggests that the amorphous shell actually decreases resistance in the system. This may either be through increased electron injection to the TiO_2 or may be through- better catalytic oxidation of the polysulfide electrolyte, the electrochemistry of which is known to be catalyzed on copper sulfide surfaces.[62,63]

Upon complete exchange to $Cu_{1.8}S$@Sn-Cu-S, the V_{oc} jumped up to 406 mV, and the J_{sc} 1.24 mA/cm². The cell characteristics are now dominated by the roxbyite $Cu_{1.8}S$ which lacks the voltage-directing core defect of the π-SnS. The J_{sc} is much improved because the band gap of roxbyite is ~1.3 compared to that of 1.7 for the π-SnS, and therefore absorbs more photons from the white light source.[64]

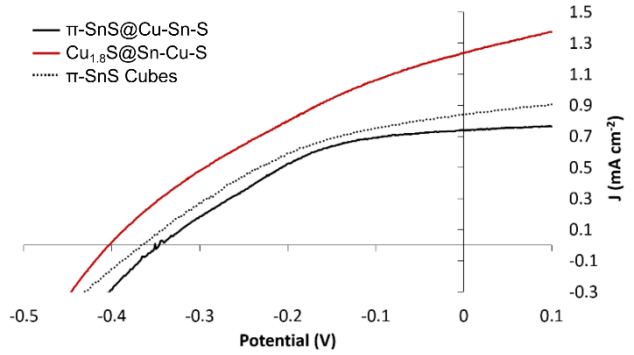

Figure 8. a) J-V curve of devices prepared using π-SnS@Cu-Sn-S (black), $Cu_{1.8}S$@Sn-Cu-S (red), and π-SnS (black dashed) nanoparticles under 1 Sun illumination (AM 1.5).

Table 1. Solar cell characteristics of liquid junction QDSSCs

Photoabsorber	V_{OC} (mV)	J_{sc} (mA cm^{-2})	FF	η (%)
SnS@Cu-Sn-S	346	0.74	0.41	0.105
$Cu_{1.8}S$@Sn-Cu-S	403	1.24	0.33	0.164

SnS cuboids	367	0.84	0.39	0.119

CONCLUSION

In this work, we show preferential phase selection in the cation exchange of cubic π-SnS to a pseudo-hexagonal $Cu_{1.8}S$ roxbyite core. Addition of Cu^{+} to π-SnS nanocuboids in solution produces several monolayers of amorphous Cu-Sn-S around the π-SnS core that became apparent only with HRTEM and EDS mapping. Raising reaction temperature results in an avalanche-like exchange of the core to products of $Cu_{1.8}S$@Sn-Cu-S core-shell nanocuboids. The inability to capture intermediates with particles that contain domains of both $Cu_{1.8}S$ and π-SnS, and the formation of voids in the products suggest that the cation exchange occurs through a "popping" of the shell followed by very fast exchange, where Sn^{2+} leaves faster than Cu^{1+} enters. The mismatched exchange kinetics are implicated as forming transient defects that catalyze the transformation of the sulfur lattice from pseudo fcc to pseudo hcp. The presence of defects during the replacement of tin forms of a cavity in the larger $Cu_{1.8}S$@Sn-Cu-S nanocuboids and is interpreted as the Kirkendall effect in nanoscale material.

The lesson to be learned is that the formation of very thin shells at intermediate steps in a cation exchange can greatly alter the diffusion kinetics in a system and thereby influence how phase is retained. It is only through carful surface analysis of intermediates, such as EDS mapping, that such a mechanism can be identified.

The particles were studied in QDSSC designs to examine how the mixed metal shell would influence the performance of π-SnS, which is an exciting new, but underperforming photoabsorber material. As expected, the cells prepared with π-SnS showed an V_{oc} of only 367 mV, which is record-breaking, but still well below the ideal given the 1.7 eV band gap of π-SnS.[30,31,60] The addition of Cu-Sn-S shells did not drastically change the cell characteristics, suggesting that the defect that is causing the low voltages is not surface associated.

ASSOCIATED CONTENT

Supporting Information includes reagent list, detailed synthetic method, UV-vis spectroscopy, transmission electron microscopy, and electron dispersion spectroscopy mapping. This material is available free of charge via the Internet at http://pubs.acs.org.

AUTHOR INFORMATION

Corresponding Author

* janet.macdonald@vanderbilt.edu

Present Addresses

† S.S.: Department of Bioengineering, University of Illinois at Urbana–Champaign, Urbana, Illinois 61801, United States and Micro and Nanotechnology Laboratory, University of Illinois at Urbana–Champaign, Urbana, Illinois 61801, United States

S.T.F.: Chemours, 1950 DuPont Rd, New Johnsonville, TN 37134

Author Contributions

The manuscript was written through contributions of all authors. All authors have given approval to the final version of the manuscript. ‡These authors contributed equally.

Funding Sources

CGS and STF would like to thank the Mitchum E. Warren fellowship. Support was provided by the U.S. National Science Foundation through NSF EPS-1004083 and NSF CHE-1905265.

Notes

Any additional relevant notes should be placed here.

ACKNOWLEDGMENT

CGS and STF would like to thank the Mitchum E. Warren fellowship. Support was provided by the U.S. National Science Foundation through NSF EPS-1004083 and NSF CHE-1905265. We thank Prof Bridget Rogers and Benjamin Schmidt for assistance with XPS analysis.

ABBREVIATIONS

XRD, powder X-ray diffraction; TEM, transmission electron microscopy; EDS, electron dispersion spectroscopy; QDSSC, Quantum Dot Sensitized Solar Cells; fcc, face centered cubic; hcp, hexagonal close packed; HAADF, high-angle annular dark-field.

REFERENCES

(1) Beberwyck, B. J.; Surendranath, Y.; Alivisatos, A. P. Cation Exchange: A Versatile Tool for Nanomaterials Synthesis. *J. Phys. Chem. C* **2013**, *117* (39), 19759–19770.

(2) Cho, G.; Park, Y.; Hong, Y. K.; Ha, D. H. Ion Exchange: An Advanced Synthetic Method for Complex Nanoparticles. *Nano Convergence*. Korea Nano Technology Research Society December 1, 2019, pp 1–17.

(3) Mohamed, M. B.; Tonti, D.; Al-Salman, A.; Chemseddine, A.; Chergui, M. Synthesis of High Quality Zinc Blende CdSe Nanocrystals. *J. Phys. Chem. B* **2005**, *109* (21), 10533–10537.

(4) Talapin, D. V.; Nelson, J. H.; Shevchenko, E. V.; Aloni, S.; Sadtler, B.; Alivisatos, A. P. Seeded Growth of Highly Luminescent CdSe/CdS Nanoheterostructures with Rod and Tetrapod Morphologies. *Nano Lett.* **2007**, *7* (10), 2951–2959.

(5) Deng, Z.; Cao, L.; Tang, F.; Zou, B. A New Route to Zinc-Blende CdSe Nanocrystals: Mechanism and Synthesis. *J. Phys. Chem. B* **2005**, *109* (35), 16671–16675.

(6) Mahler, B.; Lequeux, N.; Dubertret, B. Ligand-Controlled Polytypism of Thick-Shell CdSe/CdS Nanocrystals. *J. Am. Chem. Soc.* **2010**, *132* (3), 953–959.

(7) Sharp, C. G.; Leach, A. D. P.; Macdonald, J. E. Tolman's Electronic Parameter of the Ligand Predicts Phase in the Cation Exchange to $CuFeS_2$ Nanoparticles. *Nano Lett.* **2020**, *20* (12), 8556–8562.

(8) Norako, M. E.; Brutchey, R. L. Synthesis of Metastable Wurtzite $CuInSe_2$ Nanocrystals. *Chem. Mater.* **2010**, *22* (5), 1613–1615.

(9) Powell, A. E.; Hodges, J. M.; Schaak, R. E. Preserving Both Anion and Cation Sublattice Features during a Nanocrystal Cation-Exchange Reaction: Synthesis of Metastable Wurtzite-Type CoS and MnS. *J. Am. Chem. Soc.* **2016**, *138* (2), 471–474.

(10) Yunxia, Q.; Qiangchun, L.; Kaibin, T.; Zhenghua, L.; Zhibiao, R.; Xianming, L. Synthesis and Characterization of Nanostructured Wurtzite $CuInS_2$: A New Cation Disordered

Polymorph of $CuInS_2$. *J. Phys. Chem. C* **2009**, *113* (10), 3939–3944.
(11) Washington, A. L.; Foley, M. E.; Cheong, S.; Quffa, L.; Breshike, C. J.; Watt, J.; Tilley, R. D.; Strouse, G. F. Ostwald's Rule of Stages and Its Role in CdSe Quantum Dot Crystallization. *J. Am. Chem. Soc.* **2012**, *134* (41), 17046–17052.
(12) Ostwald, W. Studien Über Die Bildung Und Umwandlung Fester Körper. *Zeitschrift für Phys. Chemie* **1897**, *22U* (1), 289–330.
(13) Hernández-Pagán, E. A.; O'Hara, A.; Arrowood, S. L.; McBride, J. R.; Rhodes, J. M.; Pantelides, S. T.; Macdonald, J. E. Transformation of the Anion Sublattice in the Cation-Exchange Synthesis of Au_2S from $Cu_{2-x}S$ Nanocrystals. *Chem. Mater.* **2018**, *30* (24), 8843–8851.
(14) Soni, U.; Arora, V.; Sapra, S. Wurtzite or Zinc Blende? Surface Decides the Crystal Structure of Nanocrystals. *CrystEngComm* **2013**, *15* (27), 5458–5463.
(15) Gao, Y.; Peng, X. Crystal Structure Control of CdSe Nanocrystals in Growth and Nucleation: Dominating Effects of Surface versus Interior Structure. *J. Am. Chem. Soc.* **2014**, *136* (18), 6724–6732.
(16) Sahu, A.; Qi, L.; Kang, M. S.; Deng, D.; Norris, D. J. Facile Synthesis of Silver Chalcogenide (Ag_2E; E = Se, S, Te) Semiconductor Nanocrystals. *J. Am. Chem. Soc.* **2011**, *133* (17), 6509–6512.
(17) Coughlan, C.; Ibáñez, M.; Dobrozhan, O.; Singh, A.; Cabot, A.; Ryan, K. M. Compound Copper Chalcogenide Nanocrystals. *Chem. Rev.* **2017**, *117* (9), 5865–6109.
(18) Wang, L.; Guan, Z.; Tang, A. Multinary Copper-Based Chalcogenide Semiconductor Nanocrystals: Synthesis and Applications in Light-Emitting Diodes and Bioimaging. *J. Nanoparticle Res.* **2020**, *22* (1).
(19) Gui, R.; Jin, H.; Wang, Z.; Tan, L. Recent Advances in Synthetic Methods and Applications of Colloidal Silver Chalcogenide Quantum Dots. *Coord. Chem. Rev.* **2015**, *296* (October 2014), 91–124.
(20) Mu, L.; Wang, F.; Sadtler, B.; Loomis, R. A.; Buhro, W. E. Influence of the Nanoscale Kirkendall Effect on the Morphology of Copper Indium Disulfide Nanoplatelets Synthesized by Ion Exchange. *ACS Nano* **2015**, *9* (7), 7419–7428.
(21) Li, H.; Zanella, M.; Genovese, A.; Povia, M.; Falqui, A.; Giannini, C.; Manna, L. Sequential Cation Exchange in Nanocrystals: Preservation of Crystal Phase and Formation of Metastable Phases. *Nano Lett.* **2011**, *11* (11), 4964–4970.
(22) Park, J.; Zheng, H.; Jun, Y. W.; Alivisatos, A. P. Hetero-Epitaxial Anion Exchange Yields Single-Crystalline Hollow Nanoparticles. *J. Am. Chem. Soc.* **2009**, *131* (39), 13943–13945.
(23) Hodges, J. M.; Kletetschka, K.; Fenton, J. L.; Read, C. G.; Schaak, R. E. Sequential Anion and Cation Exchange Reactions for Complete Material Transformations of Nanoparticles with Morphological Retention. *Angew. Chemie - Int. Ed.* **2015**, *54* (30), 8669–8672.
(24) Steimle, B. C.; Fenton, J. L.; Schaak, R. E. Rational Construction of a Scalable Heterostructured Nanorod Megalibrary. *Science (80-.).* **2020**, *367* (6476), 418–424.
(25) De Trizio, L.; Manna, L. Forging Colloidal Nanostructures via Cation Exchange Reactions. *Chemical Reviews*. 2016, pp 10852–10887.
(26) Macdonald, J. E.; Bar Sadan, M.; Houben, L.; Popov, I.; Banin, U. Hybrid Nanoscale Inorganic Cages. *Nat. Mater.* **2010**, *9* (10), 810–815.
(27) Steimle, B. C.; Lord, R. W.; Schaak, R. E. Phosphine-Induced Phase Transition in Copper Sulfide Nanoparticles Prior to Initiation of a Cation Exchange Reaction. *J. Am. Chem. Soc.* **2020**, *142* (31), 13345–13349.
(28) Huang, J.; Kovalenko, M. V; Talapin, D. V. Alkyl Chains of Surface Ligands Affect Polytypism of CdSe Nanocrystals and Play an Important Role in the Synthesis of Anisotropic Nanoheterostructures. *J. Am. Chem. Soc.* **2010**, *132* (45), 15866–15868.
(29) Patel, M.; Kim, H. S.; Kim, J. Wafer-Scale Production of Vertical SnS Multilayers for High-Performing Photoelectric Devices. *Nanoscale* **2017**, *9* (41), 15804–15812.
(30) Ahmet, I. Y.; Guc, M.; Sánchez, Y.; Neuschitzer, M.; Izquierdo-Roca, V.; Saucedo, E.; Johnson, A. L. Evaluation of AA-CVD Deposited Phase Pure Polymorphs of SnS for Thin Films Solar Cells. *RSC Adv.* **2019**, *9* (26), 14899–14909.
(31) González-Flores, V. E.; Mohan, R. N.; Ballinas-Morales, R.; Nair, M. T. S.; Nair, P. K. Thin Film Solar Cells of Chemically Deposited SnS of Cubic and Orthorhombic Structures. *Thin Solid Films* **2019**, *672* (December 2018), 62–65.
(32) Patra, B. K.; Sarkar, S.; Guria, A. K.; Pradhan, N. Monodisperse SnS Nanocrystals: In Just 5 Seconds. *J. Phys. Chem. Lett.* **2013**, *4* (22), 3929–3934.
(33) Rabkin, A.; Samuha, S.; Abutbul, R. E.; Ezersky, V.; Meshi, L.; Golan, Y. New Nanocrystalline Materials: A Previously Unknown Simple Cubic Phase in the SnS Binary System. *Nano Lett.* **2015**, *15* (3), 2174–2179.
(34) Abutbul, R. E.; Segev, E.; Zeiri, L.; Ezersky, V.; Makov, G.; Golan, Y. Synthesis and Properties of Nanocrystalline π-SnS-a New Cubic Phase of Tin Sulphide. *RSC Adv.* **2016**, *6* (7), 5848–5855.
(35) Tu, R.; Xie, Y.; Bertoni, G.; Lak, A.; Gaspari, R.; Rapallo, A.; Cavalli, A.; Trizio, L. De; Manna, L. Influence of the Ion Coordination Number on Cation Exchange Reactions with Copper Telluride Nanocrystals. *J. Am. Chem. Soc.* **2016**, *138* (22), 7082–7090.
(36) Casavola, M.; Van Huis, M. A.; Bals, S.; Lambert, K.; Hens, Z.; Vanmaekelbergh, D. Anisotropic Cation Exchange in PbSe/CdSe Core/Shell Nanocrystals of Different Geometry. *Chem. Mater.* **2012**, *24* (2), 294–302.
(37) Lambert, K.; De Geyter, B.; Moreels, I.; Hens, Z. PbTe|CdTe Core|Shell Particles by Cation Exchange, a HR-TEM Study. *Chem. Mater.* **2009**, *21* (5), 778–780.
(38) Bouet, C.; Laufer, D.; Mahler, B.; Nadal, B.; Heuclin, H.; Pedetti, S.; Patriarche, G.; Dubertret, B. Synthesis of Zinc and Lead Chalcogenide Core and Core/Shell Nanoplatelets Using Sequential Cation Exchange Reactions. *Chem. Mater.* **2014**, *26* (9), 3002–3008.
(39) Leach, A. D. P.; Mast, L. G.; Hernández-Pagán, E. A.; Macdonald, J. E. Phase Dependent Visible to Near-Infrared Photoluminescence of $CuInS_2$ Nanocrystals. *J. Mater. Chem. C* **2015**, *3* (14), 3258–3265.
(40) Morimoto, N.; Kullerud, G. Polymorphism in Digenite. *Am. Mineral.* **1963**, *48* (November), 110–123.
(41) Zhang, J.; Chernomordik, B. D.; Crisp, R. W.; Kroupa, D. M.; Luther, J. M.; Miller, E. M.; Gao, J.; Beard, M. C. Preparation of Cd/Pb Chalcogenide Heterostructured Janus Particles via Controllable Cation Exchange. *ACS Nano* **2015**, *9* (7), 7151–7163.
(42) Mumme, G.; Gable, W. The Crystal Structure of Roxbyite, $Cu_{58}S_{32}$. *Can. Mineral.* **2012**, *50*, 423–430.
(43) Abutbul, R. E.; Golan, Y. Chemical Epitaxy of π-Phase Cubic Tin Monosulphide. *CrystEngComm* **2020**, *22* (37), 6170–6181.
(44) Yang, J. X.; Zhao, H. L.; Gong, H. R.; Song, M.; Ren, Q. Q. Proposed Mechanism of HCP → FCC Phase Transition in Titianium through First Principles Calculation and Experiments. *Sci. Rep.* **2018**, *8* (1), 23.
(45) Nair, M. T. S.; Guerrero, L.; Nair, P. K. Conversion of Chemically Deposited CuS Thin Films to Cu1.8S and Cu1.96S by Annealing. *Semicond. Sci. Technol.* **1998**, *13* (10), 1164–1169.
(46) Lee, S.; Baek, S.; Park, J. P.; Park, J. H.; Hwang, D. Y.; Kwak, S. K.; Kim, S. W. Transformation from $Cu_{2-x}S$ Nanodisks to $Cu_{2-x}S@CuInS_2$ Heteronanodisks via Cation Exchange. *Chem. Mater.* **2016**, *28* (10), 3337–3344.
(47) Rivest, J. B.; Fong, L.-K.; Jain, P. K.; Toney, M. F.; Alivisatos, A. P. Size Dependence of a Temperature-Induced Solid–Solid Phase Transition in Copper(I) Sulfide. *J. Phys. Chem. Lett.* **2011**, *2* (19), 2402–2406.
(48) Peng, Z.; Li, S.; Weng, M.; Zhang, M.; Xin, C.; Du, Z.; Zheng, J.; Pan, F. First-Principles Study of Cu_9S_5: A Novel p-Type

Conductive Semiconductor. *J. Phys. Chem. C* **2017**, *121* (42), 23317–23323.
(49) De Trizio, L.; Li, H.; Casu, A.; Genovese, A.; Sathya, A.; Messina, G. C.; Manna, L. Sn Cation Valency Dependence in Cation Exchange Reactions Involving $Cu_{2-x}Se$ Nanocrystals. *J. Am. Chem. Soc.* **2014**, *136* (46), 16277–16284.
(50) Sadtler, B.; Demchenko, D. O.; Zheng, H.; Hughes, S. M.; Merkle, M. G.; Dahmen, U.; Wang, L. W.; Alivisatos, A. P. Selective Facet Reactivity during Cation Exchange in Cadmium Sulfide Nanorods. *J. Am. Chem. Soc.* **2009**, *131* (14), 5285–5293.
(51) Ha, D. H.; Caldwell, A. H.; Ward, M. J.; Honrao, S.; Mathew, K.; Hovden, R.; Koker, M. K. A.; Muller, D. A.; Hennig, R. G.; Robinson, R. D. Solid-Solid Phase Transformations Induced through Cation Exchange and Strain in 2D Heterostructured Copper Sulfide Nanocrystals. *Nano Lett.* **2014**, *14* (12), 7090–7099.
(52) Lesnyak, V.; George, C.; Genovese, A.; Prato, M.; Casu, A.; Ayyappan, S.; Scarpellini, A.; Manna, L. Alloyed Copper Chalcogenide Nanoplatelets via Partial Cation Exchange Reactions. *ACS Nano* **2014**, *8* (8), 8407–8418.
(53) Lee, D.; Kim, W. D.; Lee, S.; Bae, W. K.; Lee, S.; Lee, D. C. Direct Cd-to-Pb Exchange of CdSe Nanorods into PbSe/CdSe Axial Heterojunction Nanorods. *Chem. Mater.* **2015**, *27* (15), 5295–5304.
(54) De Trizio, L.; Gaspari, R.; Bertoni, G.; Kriegel, I.; Moretti, L.; Scotognella, F.; Maserati, L.; Zhang, Y.; Messina, G. C.; Prato, M.; Marras, S.; Cavalli, A.; Manna, L. $Cu_{3-x}P$ Nanocrystals as a Material Platform for near-Infrared Plasmonics and Cation Exchange Reactions. *Chem. Mater.* **2015**, *27* (3), 1120–1128.
(55) Adel, P.; Wolf, A.; Kodanek, T.; Dorfs, D. Segmented CdSe@CdS/ZnS Nanorods Synthesized via a Partial Ion Exchange Sequence. *Chem. Mater.* **2014**, *26* (10), 3121–3127.
(56) Yalcin, A. O.; Fan, Z.; Goris, B.; Li, W. F.; Koster, R. S.; Fang, C. M.; Van Blaaderen, A.; Casavola, M.; Tichelaar, F. D.; Bals, S.; Van Tendeloo, G.; Vlugt, T. J. H.; Vanmaekelbergh, D.; Zandbergen, H. W.; Van Huis, M. A. Atomic Resolution Monitoring of Cation Exchange in CdSe-PbSe Heteronanocrystals during Epitaxial Solid-Solid-Vapor Growth. *Nano Lett.* **2014**, *14* (6), 3661–3667.
(57) Jain, P. K.; Amirav, L.; Aloni, S.; Alivisatos, A. P. Nanoheterostructure Cation Exchange: Anionic Framework Conservation. *J. Am. Chem. Soc.* **2010**, *132* (29), 9997–9999.
(58) Ott, F. D.; Spiegel, L. L.; Norris, D. J.; Erwin, S. C. Microscopic Theory of Cation Exchange in CdSe Nanocrystals. *Phys. Rev. Lett.* **2014**, *113* (15), 1–5.
(59) Fan, Z.; Lin, L. C.; Buijs, W.; Vlugt, T. J. H.; Van Huis, M. A. Atomistic Understanding of Cation Exchange in PbS Nanocrystals Using Simulations with Pseudoligands. *Nat. Commun.* **2016**, *7* (May 2015).
(60) Eswar Neerugatti, K. R.; Shivaji Pawar, P.; Heo, J. Differential Growth and Evaluation of Band Structure of π-SnS for Thin-Film Solar Cell Applications. *Mater. Lett.* **2021**, *284*, 129026.
(61) Finn, S. T.; Macdonald, J. E. Petaled Molybdenum Disulfide Surfaces: Facile Synthesis of a Superior Cathode for QDSSCs. *Adv. Energy Mater.* **2014**, *4* (14), 1–6.
(62) Zhao, K.; Yu, H.; Zhang, H.; Zhong, X. Electroplating Cuprous Sulfide Counter Electrode for High-Efficiency Long-Term Stability Quantum Dot Sensitized Solar Cells. *J. Phys. Chem. C* **2014**, *118* (11), 5683–5690.
(63) Hodes, G.; Manassen, J.; Cahen, D. Electrocatalytic Electrodes for the Polysulfide Redox System. *J. Electrochem. Soc.* **1980**, *127* (3), 544–549.
(64) Yong, X.; Schoonen, M. A. A. The Absolute Energy Positions of Conduction and Valence Bands of Selected Semiconducting Minerals. *Am. Mineral.* **2000**, *85* (3–4), 543–556.